Wireless Power Transfer

ARTICLE

Open Access

https://doi.org/10.48130/wpt-0024-0008

Wireless Power Transfer **2024**, 11: e006

A frequency-adjustable PCB shielding coil in Wireless Power Transfer system

Junxiang Yang, Xiangrong Zhang, Yici Wang, Shuye Shang, Kaiyuan Wang and Yun Yang*

School of Electrical and Electronic Engineering, Nanyang Technological University, Singapore

* Corresponding author, E-mail: yun.yang@ntu.edu.sg

Abstract

This paper presents the design of a frequency-adjustable PCB shielding coil for Wireless Power Transfer (WPT) systems. A simplified equivalent circuit model of the PCB coil is provided and the main parameter estimations for the PCB coil are implemented. The proposed shielding coil can reduce the electromagnetic field leakage without significantly impacting the transmission efficiency of the WPT system. Adjusting the resonant frequency of the shielding coil by changing the resonant capacitor makes it suitable for WPT systems operating at different frequencies. Experiments conducted on WPT systems operating at 100 and 200 kHz confirm the effectiveness of the shielding coil.

Citation: Yang J, Zhang X, Wang Y, Shang S, Wang K, et al. 2024. A frequency-adjustable PCB shielding coil in Wireless Power Transfer system. *Wireless Power Transfer* 11: e006 https://doi.org/10.48130/wpt-0024-0008

Introduction

Wireless Power Transfer (WPT) has garnered widespread attention due to its convenience and novelty, significantly enhancing energy transmission efficiency and increasing the product value of next-generation electronic devices and applications. Consequently, numerous issues related to WPT are currently under investigation, with electromagnetic shielding emerging as a critical topic[1]. Unlike traditional power transmission systems, WPT systems are particularly susceptible to electromagnetic interference from the environment due to their reliance on electromagnetic fields for energy transfer. Additionally, it is noteworthy that WPT systems can generate magnetic fields that may disrupt the operation of nearby electronic devices and potentially affect the health of surrounding living organisms[2,3].

To meet international standards for WPT systems and ensure personal safety, various shielding methods have been proposed to address these electromagnetic issues[4,5]. Passive shielding technology refers to the suppression of electromagnetic radiation using metal shielding materials to block the high-frequency alternating magnetic field generated by the coupling coils. This technology is the most used method for suppressing electromagnetic radiation in WPT systems. Passive shielding technology includes metal shielding[6] and magnetic material shielding[7]. In metal shielding, eddy currents generate an opposing magnetic field to counteract the stray magnetic field. Magnetic material shielding employs ferromagnetic materials to enhance the coupling coefficient between coils and provide a high-permeability channel, thereby reducing stray magnetic fields. However, for WPT systems, both methods have their respective drawbacks. The former affects the mutual inductance between the transmission coils[8], and the high conductivity of the metal plate generates eddy current losses, leading to a sharp decline in transmission efficiency[9], especially when the metal plate is placed close to the transmission coils. Although adding ferromagnetic materials can improve system efficiency and direct most of the magnetic leakage flux, the compensation capacitors or the system's operating frequency may need to be readjusted[10]. In contrast, passive coil shielding, also known as reactive power shielding, is more suitable for high-frequency WPT systems[11] (Fig. 1). Passive coil shielding uses induced currents to generate an opposing magnetic field, counteracting the stray magnetic field[12,13].

Lin et al.[4] utilized a novel W-I coupler design to electromagnetically shield the IPT system operating at 85 kHz, significantly reducing the leakage magnetic field density around the system. Meng et al.[5] employed single-sided and double-sided ferrite shielding methods, achieving maximum reductions of 41.4% and 60.5% in the target area. Pavelek et al.[13] introduced a planar reactive shield with coils and capacitors, significantly reducing the EMI level by −25.48 dB in a 6.78 MHz WPT system without compromising space or power transmission efficiency. Yan et al.[14] developed a finite element model of a wireless energy transfer system with a reconfigurable shielding plate to assess the effect of shielding on the transmission characteristics of the WPT system and thereby identify the optimal operating point and area. Hsu et al.[15] proposed three active electromotive force elimination methods—ISEC, 3DEC, and LFEC—that are highly effective in eliminating stray electromagnetic fields.

Nonetheless, adding shielding coils to the system can affect its electrical characteristics, thereby impacting the efficiency and stability of energy transmission. Therefore, the appropriate design of coil parameters is crucial to suppress electromagnetic interference and ensure stable energy transmission. Given the varying frequency requirements of different WPT systems, researching shielding coils that can easily switch between operating frequencies is essential[16]. This adaptability enhances the versatility of WPT systems, enabling efficient operation across various conditions while minimizing electromagnetic interference. Such research could result in more robust and flexible shielding solutions that cater to the diverse needs of modern WPT applications.

The AirFuel standard stipulates the use of frequencies within the Industrial, Scientific, and Medical (ISM) bands, specifically at 6.78 and 13.56 MHz[17,18]. This standard is now widely applied in consumer electronics, including Samsung smartphones, Dell laptops, and Philips wireless charging toothbrushes. Within this frequency range, PCB coils are highly favored by scholars and enterprises due to their compact size, low cost, and high manufacturing precision[18]. Concurrently, another market mainstream wireless charging standard, Qi, is widely adopted by many manufacturers, including Apple,

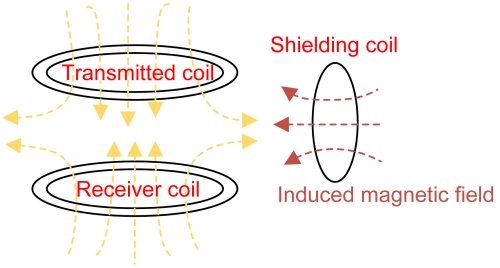

Fig. 1 Schematic diagram of reactive power shielding.

Huawei, Sony, and Microsoft. Qi standard specifies a frequency range of 100 to 205 kHz and primarily targets portable mobile phones and related products with low power levels (5~15 W). Numerous scholars are investigating WPT systems and electromagnetic field shielding methods within this frequency band[19,20]. Consequently, this paper proposes a design of a PCB shielding coil with a self-resonant frequency close to 13.56 MHz, compliant with the AirFuel standard. Additionally, the resonance frequency of coils can be adjusted to between 100 and 205 kHz using capacitors to meet the requirements of the Qi standard.

This paper proposes a self-resonant coil based on PCB with a self-resonant frequency of around 13.56 MHz, whose resonance frequency can be adjusted for electromagnetic shielding in WPT systems compliant with Qi standards. The impedance curve of the PCB coil was measured, and experiments were conducted on WPT systems operating at 100 and 200 kHz. These experiments yielded several notable findings. Firstly, at frequencies below 13.56 MHz, the skin depth of copper exceeds half the thickness of one oz copper (35 μm), indicating that the AC resistance of the coil, primarily due to the skin effect, is less than twice DC resistance. Secondly, positioning the shielding coil at specific locations within the system results in minimal impact on transmission efficiency while ensuring effective shielding. Thirdly, by identifying the lumped parameters of the coil through curve fitting, the parallel capacitor can be accurately tuned to adjust the resonance frequency. These results underscore the coil's efficacy in minimizing electromagnetic interference while maintaining optimal system performance across various frequencies.

Theoretical analysis of shielding coils for WPT systems

The equivalent circuit of the shielding coil

The designed shielding coil is shown in Fig. 2a, with its two-dimensional cross-sectional views presented in Fig. 2b. Five parameters characterize the overall shape of the coil and are utilized to adjust its resonant frequency to 13.56 MHz. The coil is a single-layer PCB coil, featuring holes in the center and at the four corners for fixation purposes. The substrate material of the coil is FR-4, and the substrate has a square shape in the top view. The parameters of the shielding coil are detailed in Table 1.

Figure 3 illustrates the equivalent circuit of the coil, comprising an inductor in series with a resistor, parallel to a resonance capacitor, thereby forming a parallel resonance structure. The inductance is determined by copper traces on the PCB, while the resistance characterizes the internal resistance of the copper. The capacitance primarily represents the collective capacitance between turns. Since losses on the shielding coil are negligible, the equivalent circuit can be simplified by omitting the resistor component, resulting in the configuration shown in Fig. 3b. According to the study by Li et al.[21], a third-order circuit is proposed to explain the equivalent circuit of the resonant coil, where both the inter-capacitance (Cs, capacitance between double-layer planar coils) and the intra-capacitance (Cp, turn-turn capacitance of a single-layer planar coil) are considered. Given that the shielding coil proposed is single-layer, the parallel LC configuration is more appropriate than the series LC configuration.

From Fig. 3a, the impedance expression for the PCB coil can be derived as:

$$Z = \frac{R}{\omega^2 C^2\left[R^2 + \left(\omega L - \frac{1}{\omega C}\right)^2\right]} + j\frac{-\frac{R^2}{\omega C} - \frac{\omega L^2}{C} + \frac{L}{\omega C^2}}{R^2 + \left(\omega L - \frac{1}{\omega C}\right)^2} \quad (1)$$

where, ω is the angular frequency. The imaginary part of the impedance can be expressed as:

$$X = \frac{-\frac{R^2}{\omega C} - \frac{\omega L^2}{C} + \frac{L}{\omega C^2}}{R^2 + \left(\omega L - \frac{1}{\omega C}\right)^2} \quad (2)$$

Let the imaginary part of the impedance equal to zero to acquire the resonant angular frequency.

$$\omega_0 = \sqrt{\frac{L - R^2 C}{CL^2}} \quad (3)$$

The skin depth is defined as:

$$\delta = \sqrt{\frac{\rho}{\pi \mu f}} \quad (4)$$

where, ρ is the electrical conductivity of copper, f is the frequency, and μ is the absolute permeability of copper. The AC resistance can be expressed as:

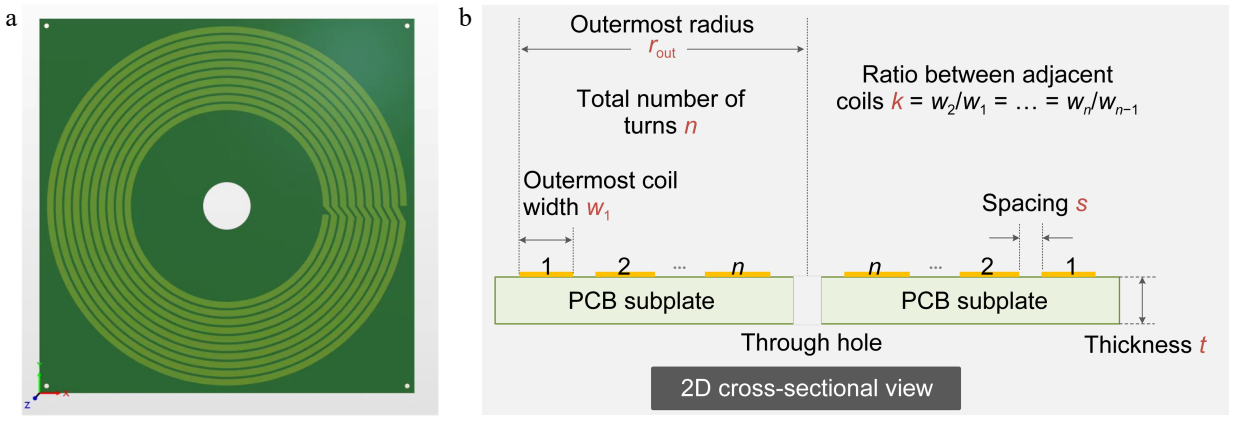

Fig. 2 Diagram of shielding coil and 2D cross-sectional view.

Table 1. Parameters of the shielding coil.

Parameters	Value
Number of turns	9
Outermost turn width	3.71 mm
Outermost radius	113.54 mm
Ratio between adjacent turns	0.999
Ratio of central hole	15 mm
Space between adjacent turns	1.75 mm
Thickness of copper	0.035 mm
Size of PCB subplate	118 mm × 118 mm × 1.6 mm
Opening angle of each turn	5°

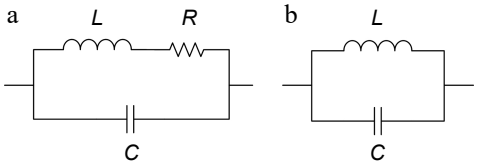

Fig. 3 The equivalent circuit of the shielding coil. (a) Complete equivalent circuit. (b) Simplified equivalent circuit.

$$R_{AC} = R_{DC} \times \frac{t}{\delta} \tag{5}$$

where, t is copper thickness. Calculations show that the skin depth at 13.56 MHz is 17.70 μm, which exceeds half the thickness of 1 oz copper (35 μm). Thus, R_{AC} is less than twice R_{DC}. The AC resistance is approximated as roughly twice the DC resistance and consider it as a constant. Additionally, with inter-turn spacing in the order of millimeters, the proximity effect can be considered negligible in comparison to the skin effect. Consequently, at operating frequencies of 13.56 MHz and below, the AC resistance of the coil can be deemed constant.

According to measurements, the coil's resistance is on the order of milliohms, whereas its inductive reactance near 100 kHz can reach the order of ohms. As the frequency increases, the inductive reactance proportionally increases. Consequently, at frequencies of 100 kHz and above, the resistance R in Fig. 3a can be neglected, leading to a simplified equivalent circuit model as depicted in Fig. 3b. This model simplifies impedance calculations, thereby facilitating subsequent parameter identification.

From the simplified equivalent circuit, the simplified impedance expression for the PCB coil can be derived as:

$$Z = \frac{j\omega L}{1 - \omega^2 LC} \tag{6}$$

The simplified imaginary part of the impedance can be expressed as:

$$X = \frac{\omega L}{1 - \omega^2 LC} \tag{7}$$

As shown in Fig. 3, the coil's self-resonance is a parallel resonance, corresponding to parallel compensation. Among the four basic compensation topologies, systems using series-series (SS) compensation and series-parallel (SP) compensation generally exhibit higher efficiency[22]. Due to disadvantages such as high input impedance, computational complexity, and dependence on the coupling coefficient and load, primary side parallel capacitor compensation is seldom used. Compared to SS compensation, SP compensation relies on the coupling factor and requires a larger primary capacitor value to achieve strong magnetic coupling. Consequently, coils with series compensation are most widely used as transmitters and receivers. Therefore, the PCB coil with a self-resonant frequency of 13.56 MHz serves as a shielding coil rather than a transmitter or receiver.

It is generally believed that the inductance of PCB coils does not change significantly (normally less than 10%) with increasing frequency (from zero Hz to around ten MHz). Therefore, the inductance measured at low frequencies is often used as a substitute for the inductance at high frequencies for analysis and calculation. To obtain a more accurate fitting value of the coil inductance at high frequencies compared to measurements at low frequencies, this study explores the use of curve fitting for parameter identification.

Electrical parameter identification

As mentioned in above, the impedance of the PCB coil was measured using an Impedance Analyzer Wayne Kerr 6500B to measure the impedance near the resonance frequency of 13.56 MHz (ranging from 10 to 18 MHz). Curve fitting was performed using the Curve Fitting Toolbox in MATLAB to determine the values of inductance and capacitance.

According to Eqn (3), neglecting the resistance, the fitting equation can be derived as follows:

$$X = \frac{2\pi Lf}{1 - \frac{f^2}{f_0^2}} \tag{8}$$

Due to the simplification of the equivalent circuit, an infinite impedance value occurs at the parallel resonance point. Therefore, the imaginary part of the impedance curve in Fig. 4 is divided into two segments on either side of the resonant frequency, and Eqn (8) is used to fit each segment to determine the inductance value. This approach ensures the convergence of the fitting process. During the simplification of the equivalent circuit model, resistance is ignored, resulting in an infinite impedance value at the resonant frequency.

According to Fig. 5 and Eqn (8), the inductance values obtained by fitting are 22.96 and 22.94 μH, respectively. The results are close, and 22.95 μH is taken as the final fitting inductance value. Comparing the fitted inductance values with those measured by the WK6500B shows only a minor discrepancy. Furthermore, adjusting the resonance frequency to specific values like 100 and 200 kHz using a parallel capacitor also verifies the accuracy of the fitted inductance values.

According to the fitting inductance L, the capacitor required to achieve a resonant frequency of 98 and 200 kHz for the shielding coil is 115 and 276 pF, respectively. After connecting the capacitor, the WK6500B was used to measure the impedance curve near 200 and 100 kHz, as shown in Fig. 6.

The final obtained inductance value of the PCB coil remains constant within the operational frequency range. Since the

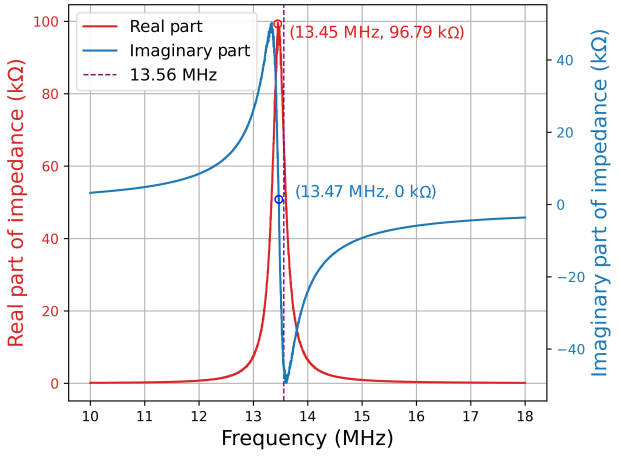

Fig. 4 Impedance of the shielded coil, including the real part and the imaginary part.

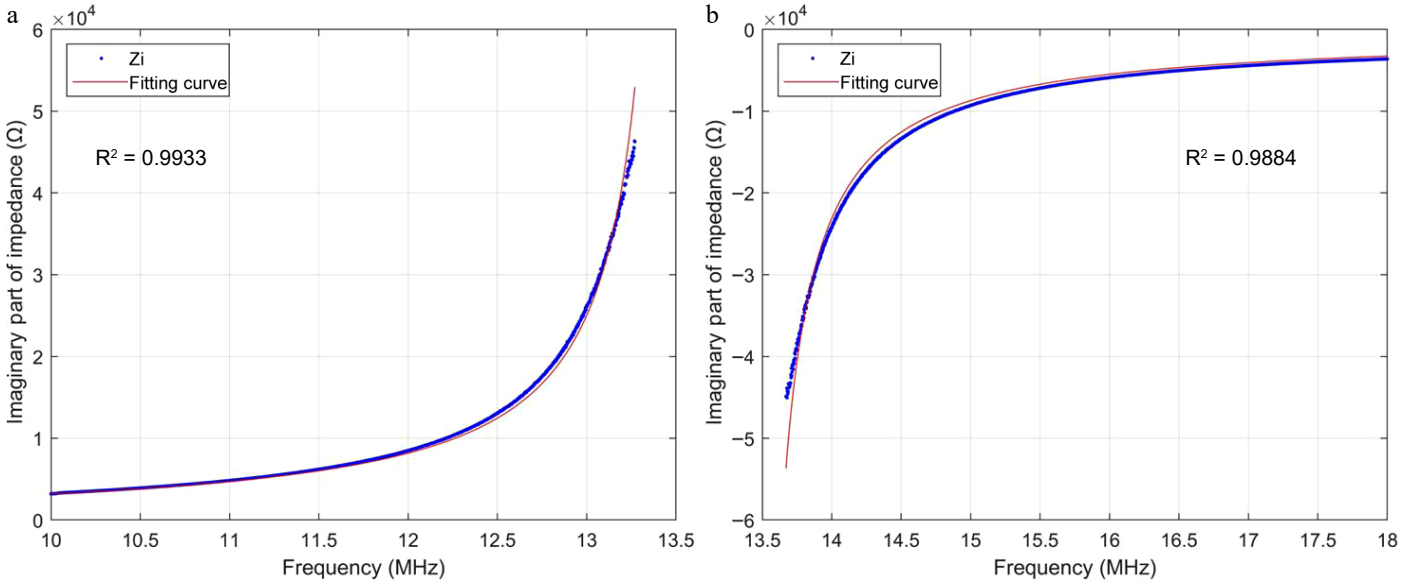

Fig. 5 Curve fitting of the imaginary part of impedance.

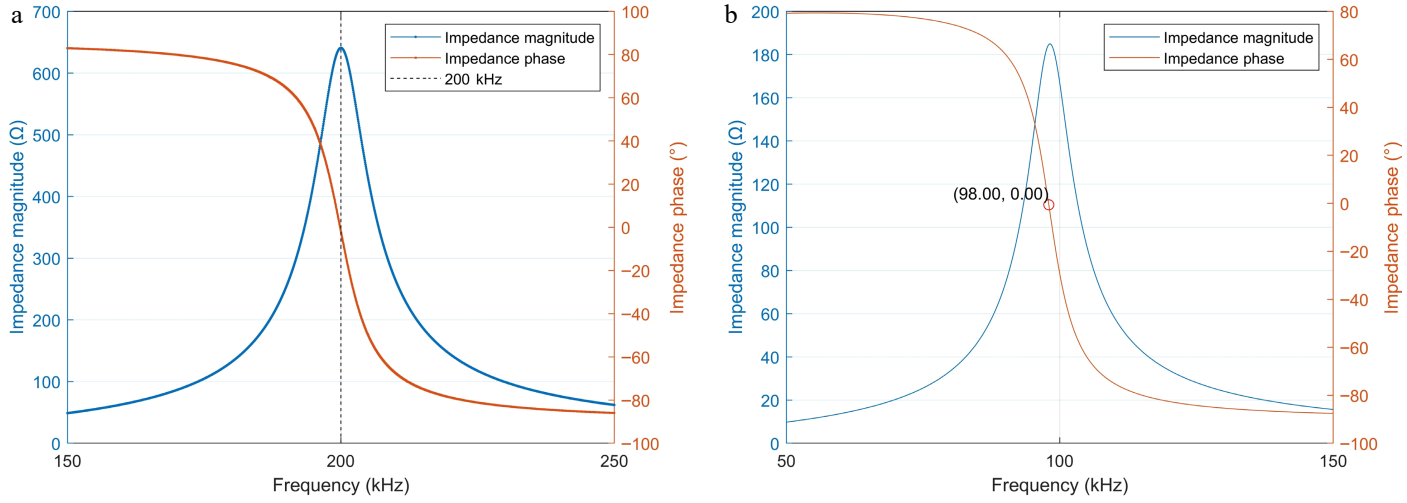

Fig. 6 Magnitude and phase of impedance of the shielding coil. (a) 200 kHz. (b) 100 kHz.

inter-turn capacitance is relatively small, and the resonance frequency is adjusted by adding capacitors in parallel, the capacitance value paralleled is at least three orders of magnitude greater than the coil's inherent capacitance when operating below one MHz. Thus, the inherent capacitance of the coil can be ignored within the WPT system.

Analysis of inductive shield in WPT system

As shown in Fig. 7, ***r*** is the displacement vector from the origin to point p, **r'** is the displacement vector from the current source to point p, ***R*** is the displacement vector from the origin to the current source, and **l'** is a loop of the annular current. According to Biot-Savart law, the magnetic induction intensive ***B*** at any point p in space generated by a current element can be expressed as:

$$\mathbf{B} = \frac{\mu_0 I}{4\pi}\int_{l'}\frac{d\mathbf{l}\times\mathbf{r}'}{\mathbf{r}'^3} = k_1 I_0 e^{j\omega t}\mathbf{e_B} \tag{9}$$

where, $I = I_0 e^{j\omega t}$ is the current. Since the magnitude of the current does not affect the direction of the magnetic field, for convenience in analysis, it is assumed that the current amplitude of the primary coil remains constant. $\mathbf{e_B}$ is the direction of the magnetic induction intensity and k_1 is the coefficient between the magnetic field and current amplitude (ensuring k_1 is positive by choosing the direction of $\mathbf{e_B}$), which depends only on the relative position of point p and the current source.

According to Faraday's law of electromagnetic induction, when the incident magnetic field generated by the WPT system is applied

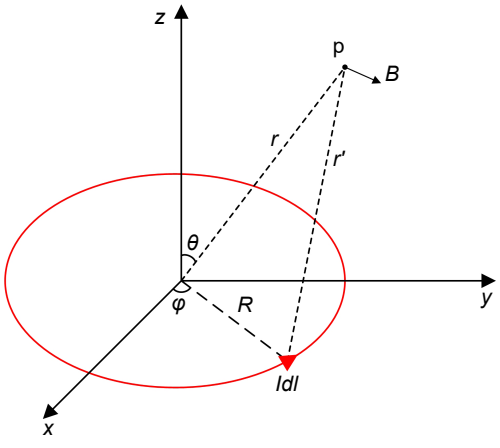

Fig. 7 Coordination system of the small loop current.

to the shielding coil, the induced voltage in one turn of the shielding coil v_i can be expressed as:

$$v_i = -\frac{\partial \Phi_{Bi}}{\partial t} = -\frac{\partial \int_{S_i} \mathbf{B} \cdot d\mathbf{A}}{\partial t} \tag{10}$$

where, Φ_{Bi} is the magnetic flux passing through the turn of the coil, **A** is the area element vector perpendicular to the coil, S_i is the area enclosed by the *i*th turn of the coil. Substituting Eqns (9) into (10) and summing over all turns yields the total induced voltage v_{sum} in the shielding coil.

$$v_{sum} = \sum_i^n v_i = -j\omega I_0 e^{j\omega t} \sum_i^n k_1 \mathbf{e_B} \cdot \mathbf{S_i} = -j\omega k_2 I_0 e^{j\omega t} \tag{11}$$

where, $\mathbf{S_i}$ is the oriented area of each turn of the coil, and k_2 is a constant coefficient that depends only on the relative position of the shielding coil and the WPT system (ensuring k_2 is positive by choosing the direction of $\mathbf{S_i}$). It can be observed that the phase of the induced electromotive force generated by the shielding coil differs by 90° from the combined magnetic field generated by the transmitter and receiver. Next, the impact of the shielding coil impedance on the magnetic shielding effect is examined. By controlling the matching capacitors, the resonance frequency of the coil can be changed, thereby determining whether the shielding coil exhibits capacitive or inductive impedance at the operating frequency. The impedance and current of the shielding coil can be expressed as:

$$Z_S = R_S + j\left(\omega L_S - \frac{1}{\omega C_S}\right) \tag{12}$$

$$i_S = \frac{v_{sum}}{Z_S} = \frac{v_{sum}}{R_S + j\left(\omega L_S - \frac{1}{\omega C_S}\right)} \tag{13}$$

At the resonance frequency point, the shielding current can be expressed as:

$$i_S = \frac{v_{sum}}{R_S} \tag{14}$$

According to Eqns (9)–(14), the magnetic field generated by the shielding coil can be expressed as:

$$B' = \frac{-j\omega k'_1 k_2 I_0 e^{j\omega t}}{R_S} \mathbf{e_{B'}} \tag{15}$$

where, $\mathbf{e_{B'}}$ is related to the position of the shielding coil, but it always forms an acute angle with $\mathbf{e_B}$. The magnetic field generated by the shielding coil always lags 90° behind the magnetic field generated by the WPT system.

In the inductive region, the shielding current can be expressed as:

$$i_S = \frac{v_{sum}}{R_S + j\omega L_S} \tag{16}$$

Assuming R_S is much less than ωL_S, the magnetic field **B'** generated by the shielding coil can be expressed as:

$$\mathbf{B'} = -\frac{k_1' k_2 I_0 e^{j\omega t}}{L_S} \mathbf{e_{B'}} \tag{17}$$

The magnetic field generated by the shielding coil can counteract the magnetic field produced by the WPT system at any point in space.

In the capacitive region, the shielding current can be expressed as:

$$i_S = \frac{v_{sum}}{R_S - j\frac{1}{\omega C_S}} \tag{18}$$

Assuming R_S is much less than $1/(\omega C_S)$, the magnetic field **B'** generated by the shielding coil can be expressed as:

$$\mathbf{B'} = k_1' k_2 \omega^2 C_S I_0 e^{j\omega t} \mathbf{e_{B'}} \tag{19}$$

The generated magnetic field component is in the same direction as the original magnetic field, thus enhancing the original magnetic field. However, adding the shielding coil will change the mutual inductance between the transmitting and receiving coils, so it cannot be simply assumed that the magnetic field will increase or decrease. To clarify this issue further, the next section will introduce an equivalent circuit model to explain the shielding mechanism when the shielding coil is in the capacitive region.

Analysis of capacitive shield in WPT system

Without any external load or power supply, the shielding coil operates as a series resonance in this system, as shown in Fig. 8.

The equivalent circuit diagram of the WPT system is shown in Fig. 8. As shown in Fig. 8a, L_1, L_2, and L_S are the self-inductance of the source, load, and shielding coil, respectively. C_1, C_2, and C_S are the compensation capacitors accordingly. It is important to note that C_S represents an external capacitor, instead of the capacitor *C* shown in Fig. 3. ω_0 is the resonant angular frequency of the system, and it has been defined as Eqn (20) according to Eqn (3). The resonance frequency of the shielding coil is different from the operating frequency of the system ω_0.

$$\omega_0 = 2\pi f_0 = \frac{1}{\sqrt{L_1 C_1}} = \frac{1}{\sqrt{L_2 C_2}} \tag{20}$$

In Fig. 8, R_1 and R_S are the parasitic resistance of the transmitting coil and shielding coil, respectively. Since the resistance of the load R_L (around 10 Ω) is much larger than the parasitic resistance of the receiving coil (less than 10 mΩ), the parasitic resistance of the receiving coil can be neglected, as shown in Fig. 8. M_{12}, M_{1S}, M_{2S} are the mutual inductance of these three coils. *v* is the output voltage of the inverter. Additionally, i_1, i_2, and i_S are the currents of the coils in the

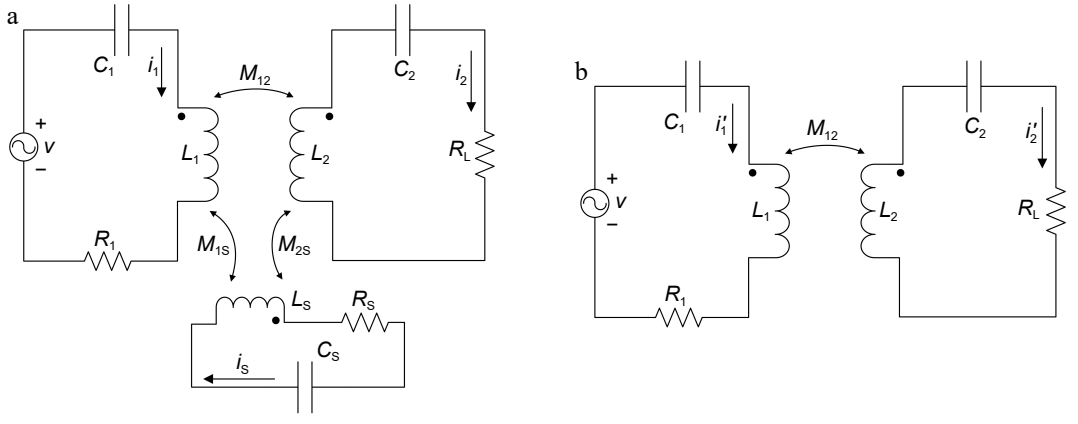

Fig. 8 Circuit structure of the WPT system: (a) with a shielding coil, (b) without a shielding coil.

WPT system with a shielding coil, while i_1' and i_2' are the currents of transmitter and receiver coils in the system without a shielding coil.

With the lumped-element circuit shown in Fig. 8a, the WPT system can be expressed in the matrix form according to Kirchhoff voltage law (KVL) as follows:

$$\begin{bmatrix} v \\ 0 \\ 0 \end{bmatrix} = \begin{bmatrix} Z_1 & j\omega_0 M_{1S} & j\omega_0 M_{12} \\ j\omega_0 M_{1S} & Z_S & j\omega_0 M_{2S} \\ j\omega_0 M_{12} & j\omega_0 M_{2S} & Z_2 \end{bmatrix} \begin{bmatrix} i_1 \\ i_S \\ i_2 \end{bmatrix} \tag{21}$$

where,

$$Z_i = R_i + j\omega_0 L_i - \frac{j}{\omega_0 C_i} \tag{22}$$

where, v is the voltage vector of the equivalent AC input power supply, and Z_i (i = 1, 2, or S) represents the impedance of the three coils, respectively. Since the coils are resonant, the imaginary part of Z_i should be zero. By Gaussian elimination, Eqn (21) is simplified as:

$$\begin{bmatrix} Z_1 + \frac{(\omega_0 M_{1S})^2}{Z_S} & \mathrm{j}\omega_0 \left(M_{12} - \mathrm{j}\omega_0 \frac{M_{1S} M_{2S}}{Z_S} \right) \\ \mathrm{j}\omega_0 \left(M_{12} - \mathrm{j}\omega_0 \frac{M_{1S} M_{2S}}{Z_S} \right) & Z_2 + \frac{(\omega_0 M_{2S})^2}{Z_S} \end{bmatrix} \begin{bmatrix} i_1 \\ i_2 \end{bmatrix} = \begin{bmatrix} v \\ 0 \end{bmatrix} \tag{23}$$

According to Eqn (23), the equivalent mutual inductance between the transmitting coil and receiving coil M_{12}', as well as their respective equivalent impedances (Z_1' and Z_2') after adding the shielding coil, can be expressed as:

$$M_{12}' = M_{12} - \mathrm{j}\omega_0 \frac{M_{1S} M_{2S}}{Z_S} \tag{24}$$

$$Z_1' = Z_1 + \frac{(\omega_0 M_{1S})^2}{Z_S} \tag{25}$$

$$Z_2' = Z_2 + \frac{(\omega_0 M_{2S})^2}{Z_s} \tag{26}$$

The equivalent currents of the transmitting coil and the receiving coil in WPT system with a shielding coil can be expressed as:

$$\begin{cases} i_1 = \dfrac{v Z_2'}{Z_1' Z_2' + (\omega_0 M_{12}')^2} \\ i_2 = \dfrac{j\omega_0 v M_{12}'}{Z_1' Z_2' + (\omega_0 M_{12}')^2} \end{cases} \tag{27}$$

The equivalent currents of the transmitting coil and the receiving coil in WPT system without a shielding coil can be expressed as:

$$\begin{cases} i_1' = \dfrac{v Z_2}{R_1 R_L + (\omega_0 M_{12})^2} \\ i_2' = \dfrac{j\omega_0 v M_{12}}{R_1 R_L + (\omega_0 M_{12})^2} \end{cases} \tag{28}$$

When the shielding coil impedance is capacitive, it can be represented by an equivalent capacitance.

$$Z_S = \frac{1}{j\omega_0 C_{eq}} \tag{29}$$

Substituting Eqn (29) into Eqns (24)–(26).

$$M_{12}' = M_{12} \left(1 + \frac{\omega_0^2 M_{1S} M_{2S} C_{eq}}{M_{12}} \right) \tag{30}$$

$$Z_1' = Z_1 + j\omega_0^3 C_{eq} M_{1S}^2 \tag{31}$$

$$Z_2' = Z_2 + j\omega_0^3 C_{eq} M_{2S}^2 \tag{32}$$

According to Eqns (31) and (32), the equivalent impedance of the transmitting coil and the receiving coil increases. Additionally, the mutual inductance can be expressed in terms of the coupling coefficient ($k_{ab} = M_{ab} / \sqrt{L_a L_b}$) as:

$$\begin{cases} M_{1S} = k_{1S} \sqrt{\dfrac{L_1}{C_{\mathrm{eq}}}} \\ M_{12} = k_{12} \sqrt{L_1 L_2} \\ M_{2S} = k_{2S} \sqrt{\dfrac{L_2}{C_{\mathrm{eq}}}} \end{cases} \tag{33}$$

where, k_{1S}, k_{2S}, and k_{12} are the coupling coefficients between the transmitter and the shielding coil, the receiver and the shielding coil, and the transmitter and the receiver, respectively. Therefore, after adding the shielding coil, the system's equivalent mutual inductance and equivalent coupling coefficient can be expressed as:

$$M_{12}' = M_{12} \left(1 + \frac{\omega_0^2 k_{1S} k_{2S}}{k_{12}} \right) \tag{34}$$

$$k_{12}' = k_{12} + \omega_0^2 k_{1S} k_{2S} \tag{35}$$

According to Eqn (35), when the shielding coil impedance is in the capacitive region, the equivalent coupling coefficient between the transmitting coil and the receiving coil in the system with the shielding coil is higher compared to the system without the shielding coil. This enhances the magnetic field between the coils, consistent with the conclusion above.

According to Eqn (29), since the magnitude of the impedance of shielding coil is larger than 10 Ω, it is reasonable to believe that $C_{\mathrm{eq}} < \omega_0 / 10$. Assuming R_L is much larger than $\omega_0^3 C_{eq} M_{2S}^2$, according to Equation (22) and Eqn (32), $Z_2' = Z_2 = R_L$. Substituting it into Eqns (27) and (28), it is clear that $i_1 < i_1'$. Next, we will determine the relationship between i_2 and i_2'. We define the ratio of i_2 to i_2' as α, which can be expressed as:

$$\alpha = \frac{i_2}{i_2'} = \frac{M_{12}\beta + \omega_0^2 M_{1S} M_{2S} C_{eq} \beta}{M_{12}\beta + j\omega_0^3 C_{eq} M_{12} M_{1S}^2 R_L} \tag{36}$$

where,

$$\beta = R_1 R_L + \omega_0^2 M_{12}^2 \tag{37}$$

According to Eqns (36) and (37), the relationship between α and 1 depends on γ:

$$\gamma = \frac{\omega_0^2 M_{1S} M_{2S} C_{eq} \beta}{\omega_0^3 C_{eq} M_{12} M_{1S}^2 R_L} = \frac{R_1 R_L + \omega_0^2 M_{12}^2}{\omega_0 M_{1S} R_L} \tag{38}$$

According to Eqn (33) and the quality factor of the transmitter $Q_1 = \omega_0 L_1 / R_1$, and assuming L_S is close to L_1 and L_2, γ also can be expressed as:

$$\gamma = \frac{R_L / Q_1 + \omega_0 k_{12}^2 L_2}{k_{1S} R_L} \tag{39}$$

where, the reference range for the quality factor Q_1 of the transmitting coil is 100 to 400, R_{L} is around 10 Ω, the reference range for k_{12} and k_{1S} is 0.1 to 0.4, L_2 is approximately 50 μH. We estimate $\gamma < 1$ at the reference magnitude, as shown in Fig. 9. Therefore, α is also less than one at the reference magnitude, which means $i_2 < i_2'$. According to Eqn (9), the current magnitude is proportional to the magnetic induction intensity. The parameters used in the estimation process are shown in Table 2. The magnetic fields generated by the transmitting coil and the receiving coil decrease, resulting in an overall reduction of the leakage magnetic field.

Next, the losses in the shielding coil are considered. The shielding coil operates at or very close to its series resonance frequency in the WPT system. Therefore, the losses in the shielding coil can be primarily attributed to the parasitic resistance of shielding coil R_S. The losses can be calculated using Joule's law. According to Fig. 8 and Eqn (21), the current of shielding coil i_S and receiver coil i_2 can be expressed as:

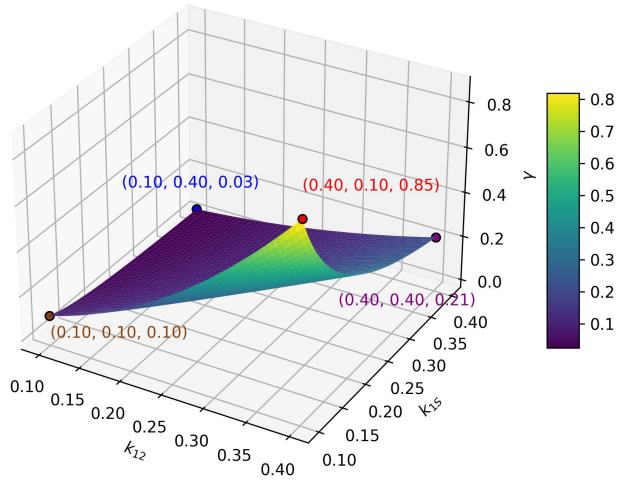

Fig. 9 γ in different k_{12} and k_{1S}.

Table 2. Parameters used in Figs 9 & 10.

Parameters	Value
Load R_L	10 Ω
Quality factor of transmitter Q_1	200
Inductance L_2	50 μH

$$i_S = \frac{-(M_{12}M_{2S}\omega_0^2 + j\omega_0 M_{1S}R_2)u}{k} \tag{40}$$

$$i_2 = \frac{-(j\omega_0 M_{12}R_S + M_{1S}M_{2S}\omega_0^2)}{k}u \tag{41}$$

where,

$$k = M_{12}^2R_S\omega_0^2 - 2j\omega_0^3M_{12}M_{1S}M_{2S} + M_{1S}^2R_2\omega_0^2 + M_{2S}^2R_1\omega_0^2 + R_1R_2R_S \tag{42}$$

The losses in the shielding coil Q_S and power in receiver coil P can then be represented as:

$$Q_S = |i_S|^2R_S \tag{43}$$

$$P = |i_2|^2R_2 \tag{44}$$

Since $M_{1S}^2R_2\omega_0^2$ is much larger than $M_{12}^2R_S\omega_0^2 + M_{2S}^2R_1\omega_0^2 + R_1R_2R_S$, and $M_{1S}M_{2S}\omega_0^2$ is much larger than $\omega_0 M_{12}R_S$, the ratio of losses and power can be expressed as:

$$\frac{Q_S}{P} = \frac{|i_S|^2R_S}{|i_2|^2R_2} = \frac{(M_{12}^2M_{2S}^2\omega_0^4 + \omega_0^2M_{1S}^2R_2^2)R_S}{M_{1S}^2M_{2S}^2\omega_0^4R_2} \tag{45}$$

Through estimates similar to those in Eqn (38) and Eqn (39), we can determine that $M_{12}^2M_{2S}^2\omega_0^4 + \omega_0^2M_{1S}^2R_2^2$ and $M_{1S}^2M_{2S}^2\omega_0^4$ are of the same order of magnitude, while R_S is much less than R_2. Therefore, when the shielding coil is not placed too close to the Tx or Rx coils, the losses on it can be considered relatively small.

Shielding effect of the shielding coil in resonance

When the shielding coil operates in resonance, its impedance can be expressed as $Z_S = R_S$. According to Eqns (21)–(28), the ratio of $|i_2|$ to $|i_2'|$ can be expressed as:

$$|\alpha| = \frac{\left|M_{12} - j\omega_0\frac{M_{1S}M_{2S}}{R_S}\right|\beta}{M_{12}\left|\left(R_1 + \frac{\omega_0^2M_{1S}^2}{R_S}\right)\left(R_L + \frac{\omega_0^2M_{2S}^2}{R_S}\right) + \omega_0^2\left(M_{12} - j\omega_0\frac{M_{1S}M_{2S}}{R_S}\right)^2\right|} \tag{46}$$

Since $|\omega_0 M_{1S}M_{2S}/R_S|$ is much larger than $|M_{12}|$, R_1 is much less than $\omega_0^2M_{1S}^2/R_S$, $\omega_0^2M_{1S}^2R_L$ is much larger than $2\omega_0^3M_{12}M_{1S}^2M_{2S}^2$ and $\omega_0 M_{12}M_{1S}R_L$ is much larger than $\omega_0 M_{12}^3R_S$, $|\alpha|$ can be expressed as:

$$|\alpha| = \frac{M_{2S}(R_1R_L + \omega_0^2M_{12}^2)}{\omega_0 M_{12}M_{1S}R_L} = \frac{\frac{R_Lk_{2S}}{Q_1} + \omega_0k_{12}^2k_{1S}L_2}{k_{12}k_{1S}R_L} \tag{47}$$

We estimate the value of $|\alpha|$ within the same reference range as above. The parameters used in the estimation process are also shown in Table 2. As shown in Fig. 10, $|\alpha|$ is always less than 1, which means that the shielding coil operating at the resonance frequency also has a shielding effect.

Simulation and experimental investigation based on WPT systems

Simulation of electromagnetic fields in WPT systems

Finite element electromagnetic field simulations are conducted using Ansys Maxwell software to explore the shielding effect of the shielding coil on the axial magnetic field in both WPT systems with and without the shielding coil.

According to Fig. 11, in the WPT system without the shielding coil, the magnetic flux density at the observation points remains around 80 μT. After adding the shielding coil, the magnetic flux density at the observation points drops significantly below 60 μT in a large portion of the area, and the overall magnetic flux density is reduced. The simulation results preliminarily verify the shielding effect of the shielding coil on the electromagnetic field in the WPT system.

Shielding effect experiment setup

Experiments were conducted on two WPT systems operating at different frequencies to explore the effects of the shielding coil on the systems' magnetic field and transmission efficiency. In the first set of experiments (Experiment A), the resonance frequency of transmitter and receiver was set to 100 kHz, while in the second set (Experiment B), it was set to 200 kHz. In Experiment A, the resonance frequency of the shielding coil was set to 98 kHz, which means that it worked in the inductive region. In Experiment B, the resonance frequency of the shielding coil was adjusted to match the resonance frequencies of the WPT system's transmitting and receiving coils.

As shown in Fig. 12, the WPT systems used in the experiments consist of transmitting and receiving coils (Tx coil and Rx coil) that utilize series capacitance compensation, while the shielding coil

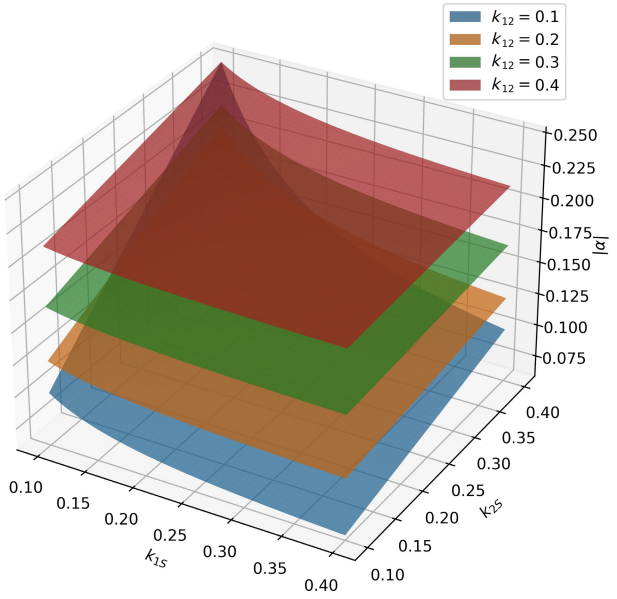

Fig. 10 $|\alpha|$ in different k_{12}, k_{1S}, and k_{2S}.

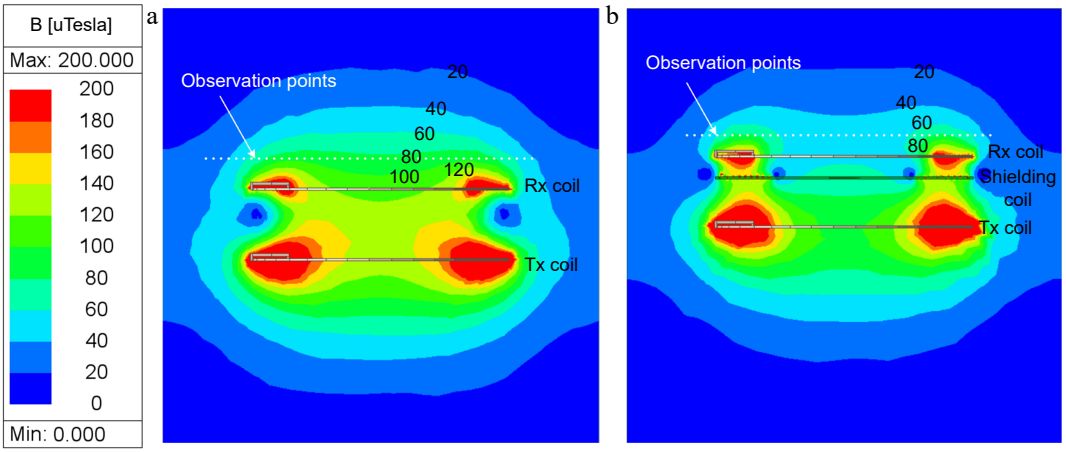

Fig. 11 Distribution of the simulated magnetic field: (a) without, (b) with the resonant reactive shield.

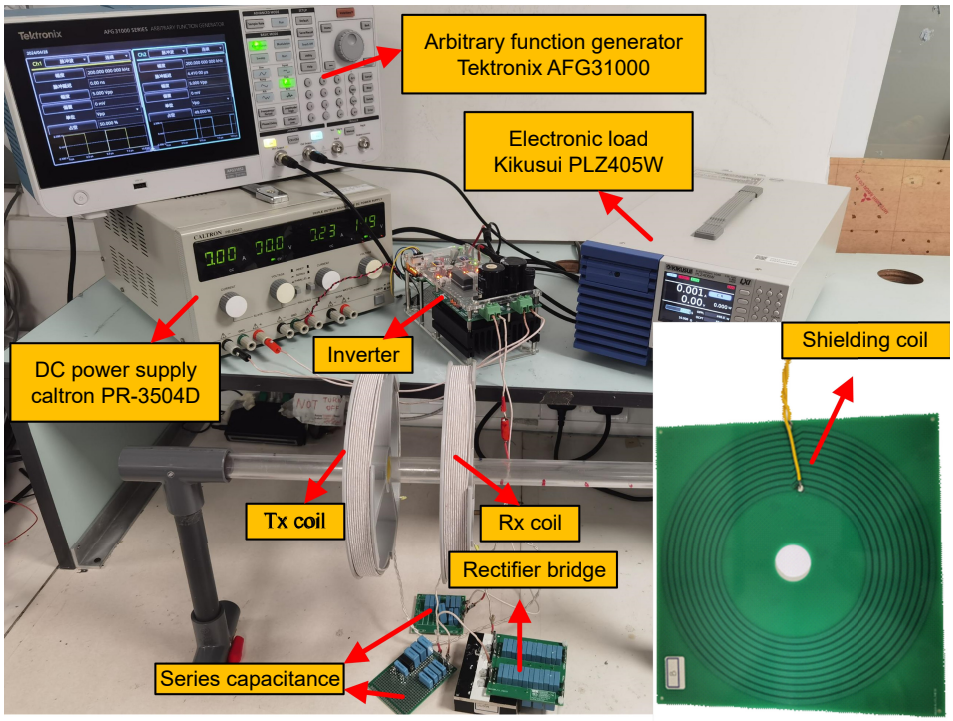

Fig. 12 Photograph of the experiment setup.

employs parallel capacitance to adjust to the corresponding resonance frequency. The inverter is powered by a DC power supply, and an arbitrary function generator provides the driving waveform (a pulse wave corresponding to the resonant frequency) to the inverter. The alternating current from the receiving coil is connected to the electrical load through a rectifier bridge. The main parameters of the system are shown in Table 3.

In the experiments, two placement schemes for the shielding coil were tested: one parallel to the transmitting and receiving coils, and the other perpendicular to them. Using the transmitting coil as the coordinate origin, the shielding coil was positioned at various distances from the transmitting coil, and the output power and transmission efficiency of the system were measured.

As shown in Fig. 13, there are eight test placement schemes for shielding coils parallel to the transmitting coil (Cases a to h). Case a serves as a control group without a shielding coil. Additionally, the output power of the receiving coil and the input power of the transmitting coil were measured to calculate the efficiency across the resonator.

As shown in Fig. 14, the distance between the center of the shielding coil and the Tx coil is defined as x, ranging from −16 to

Table 3. Parameters for WPT system used in the experiments.

Parameters	Value
Operation frequency of Experiment A	100 kHz
Operation frequency of Experiment A	200 kHz
Number of turns of Tx and Rx coils	11
Radius of Tx coil and Rx coil	10 cm
Load	10 Ω
Inductance of Tx coil	47.52 μH
Inductance of Rx coil	47.75 μH
Series capacitance of Tx coil in Experiment A	53.30 nF
Series capacitance of Rx coil in Experiment A	53.05 nF
Series capacitance of Tx coil in Experiment B	13.33 nF
Series capacitance of Rx coil in Experiment B	13.26 nF
Distance between Tx coil and Rx coil	6.5 cm
Mutual induction of Tx coil and Rx coil	9.847 μH
Wire diameter of Tx coil and Rx coil	1.8 mm

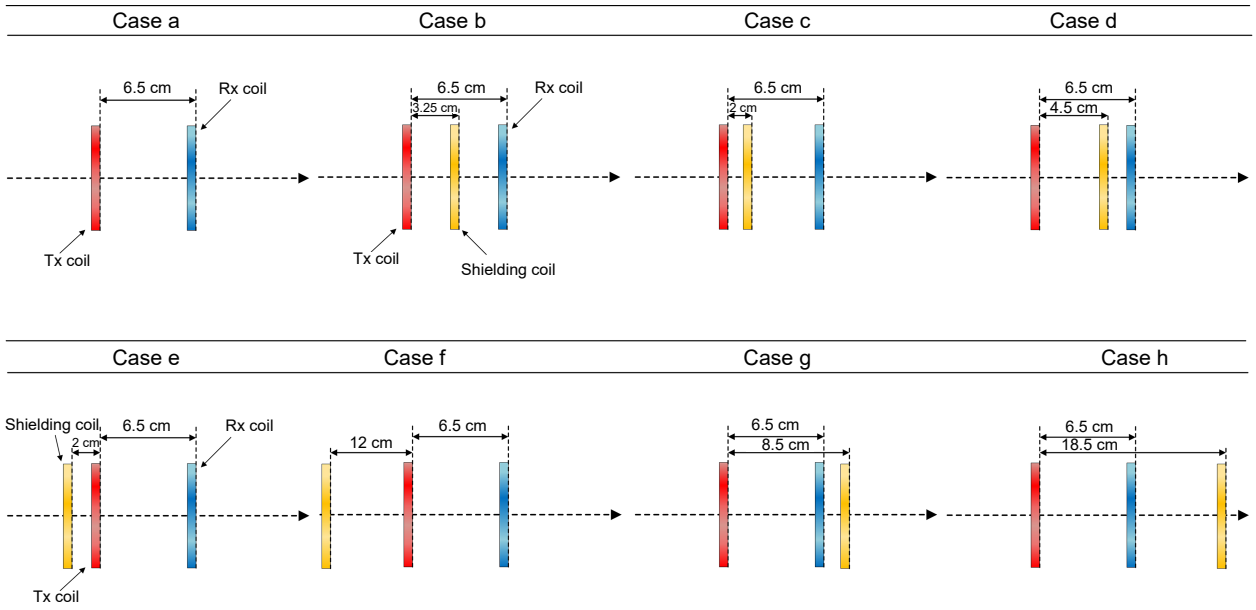

Fig. 13 Schematic diagram of shielding coil placed in different positions (parallel to the transmitting coil).

14 cm. Additionally, by placing the shielding coil on a straight line perpendicular to the transmitting coil and 2 cm away from it, a set of experimental data was obtained to test the shielding effect on side magnetic leakage.

Results of Experiment A

This section focuses on the impact of introducing the shielding coil and placing it in different positions on the transmission efficiency and output power of the system. Figure 15 shows the transmission efficiency at both ends of the transmitting coil and the receiving coil, as well as the output power at the receiving coil, with the horizontal axis representing the power supply voltage. The four curves in the figure can be divided into two groups: one group represents the resonator (the two ends of the resonant coils), and the other group represents the entire WPT system. Analyzing the structure of the entire system reveals that the difference between these two losses mainly arises from the rectifier and inverter.

From Fig. 16, it is evident that placing the shielding coil parallel to the transmitting coil at different positions has varying effects on the system's transmission efficiency and output power. According to previous theoretical analysis, the shielding effect of the coil is evaluated by the amplitude of the secondary current, which is closely related to the output power. Based on Fig. 16, in Case h, the output power does not decrease significantly, and there is a situation where the primary current becomes too large, causing the inverter to fail. Although Cases c and e effectively reduce output power, they also severely impact the system's transmission efficiency. When the shielding coil is placed between the transmitting and receiving coils, two cases—Case b and Case d—are able to effectively reduce output power while minimizing the impact on transmission efficiency. When the shielding coil is placed outside the transmission coils, Case f shows the best overall shielding effect. It is worth noting that the results of Experiment A validate the shielding effect of the shielding coil when its resonant frequency is in the inductive region.

From Fig. 17, it is evident that placing the shielding coil perpendicular to the transmitting coil results in a reduction in both transmission efficiency and output power compared to the system without a shielding coil. However, the extent of this reduction varies depending on the specific placement. These effects can be summarized as follows:

(1) The most significant decreases in transmission efficiency and output power occurs approximately −10 to −6 cm and 6 to 8 cm away from the transmitting coil. Given that the outer diameter of the shielding coil is about 11 cm, it can be inferred that at these distances, roughly half of the shielding coil is adjacent to the transmitting coil, where the eddy current effect is most significant. Therefore, shielding coils positioned at these locations have the greatest impact on the normal operation of the WPT system.

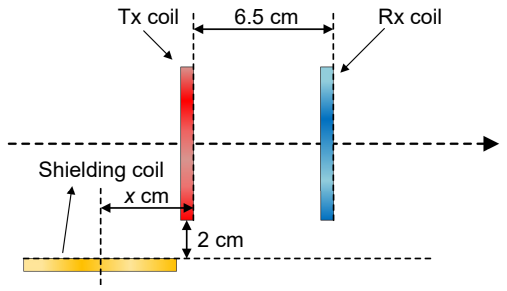

Fig. 14 Schematic diagram of the shielding coil (perpendicular to the transmitting coil).

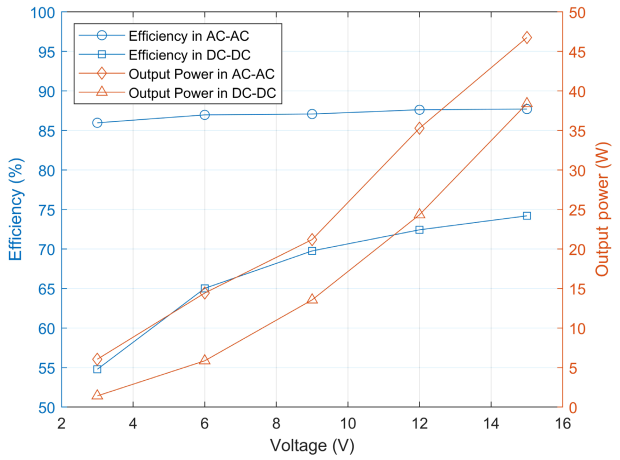

Fig. 15 Efficiency between resonator or WPT system and output power of Rx coil or rectifier bridge in Experiment A.

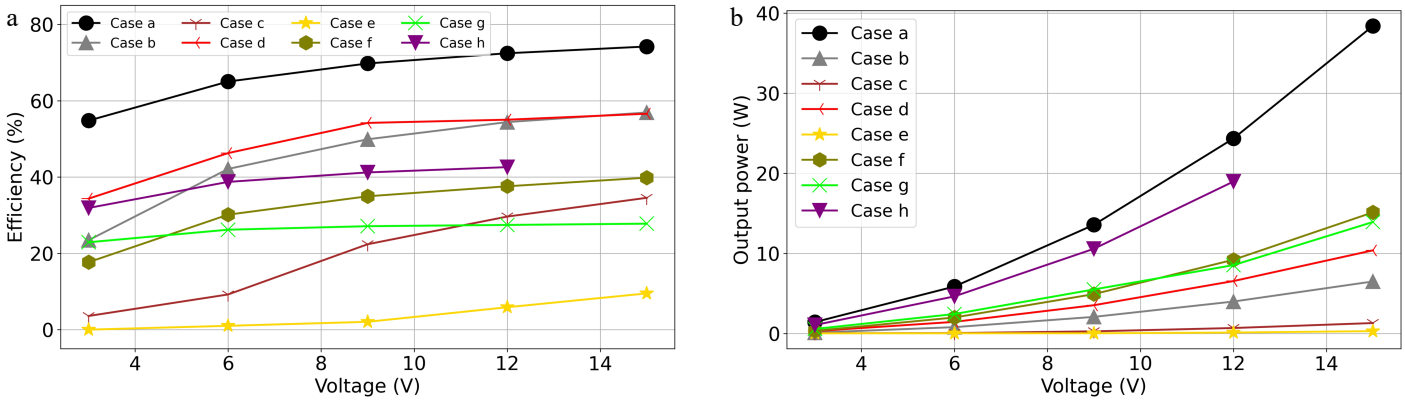

Fig. 16 (a) Efficiencies, and (b) output powers of the WPT system in Experiment A from Case a to h.

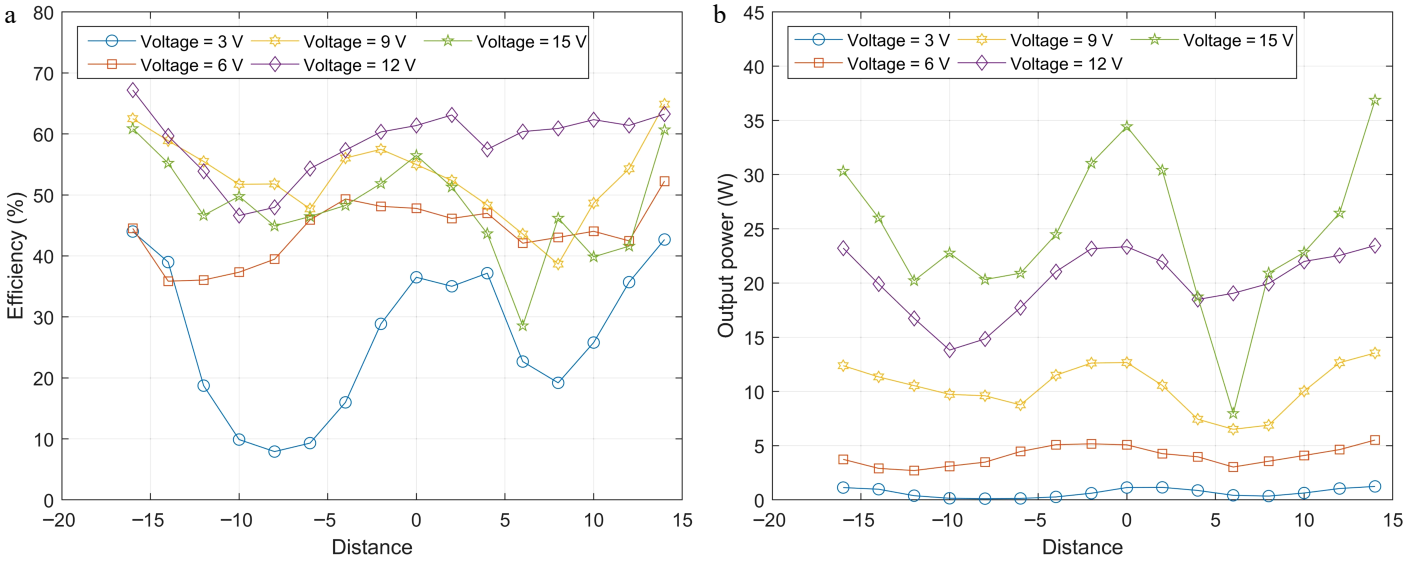

Fig. 17 (a) Efficiencies, and (b) output powers of the WPT system at different voltages in Experiment A when the shielding coil is perpendicular to the transmitting coil.

(2) At locations far away from the transmitting coil, the transmission efficiency and output power are comparable to those observed without a shielding plate.

(3) Between x = −2 to 0 cm, the output power reaches its peak, while between x = 0 to 2 cm, the transmission efficiency peaks. Therefore, placing a shielding coil between the transmitting coil and the receiving coil can achieve a more effective shielding effect.

Results of Experiment B

As shown in Fig. 18, 19 and 20, it is noticeable that placing the shielding coil perpendicular to the transmitting coil yields similar conclusions to Experiment A. Since the shielding coil is at the resonance frequency in Experiment B, it can be demonstrated that there is a shielding effect under this condition also. Among the various cases, Case b demonstrates the best overall shielding effect, not only reducing output power but also having a lower impact on efficiency compared to the other cases.

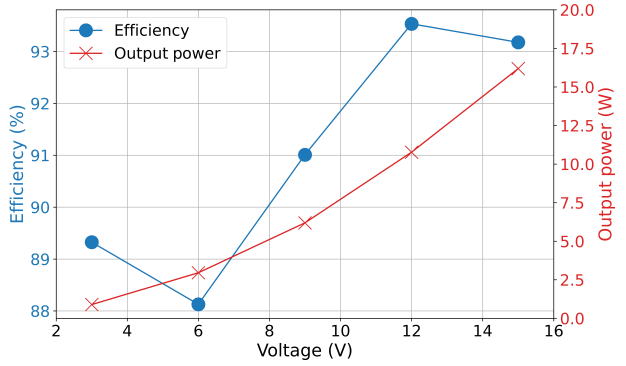

Fig. 18 Efficiency between resonator or WPT system and output power of Rx coil or rectifier bridge in Experiment B.

Conclusions

This paper presents a design for a frequency-adjustable PCB shielding coil tailored for WPT systems operating at various frequencies. The operational frequency of the coil is adjusted by changing the value of the parallel capacitance. By fitting the value of inductance, the optimal parallel capacitance is determined. Experimental results demonstrate that the shielding coil effectively reduces electromagnetic interference while maintaining high transmission efficiency in WPT systems. This highlights the effectiveness of the proposed design in enhancing the functionality and adaptability of shielding solutions for WPT applications.

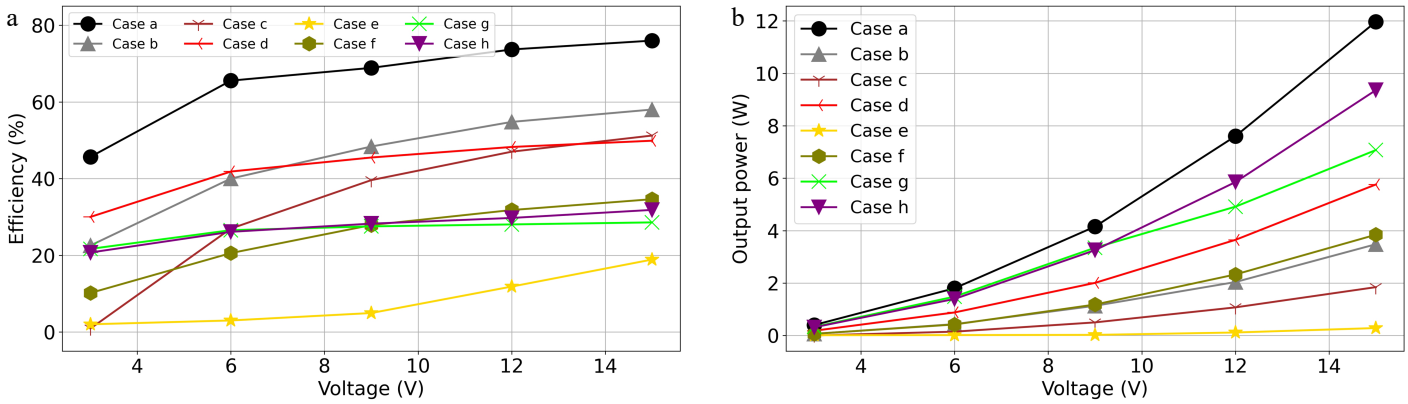

Fig. 19 (a) Efficiencies, and (b) output powers of the WPT system in Experiment B from Case a to h.

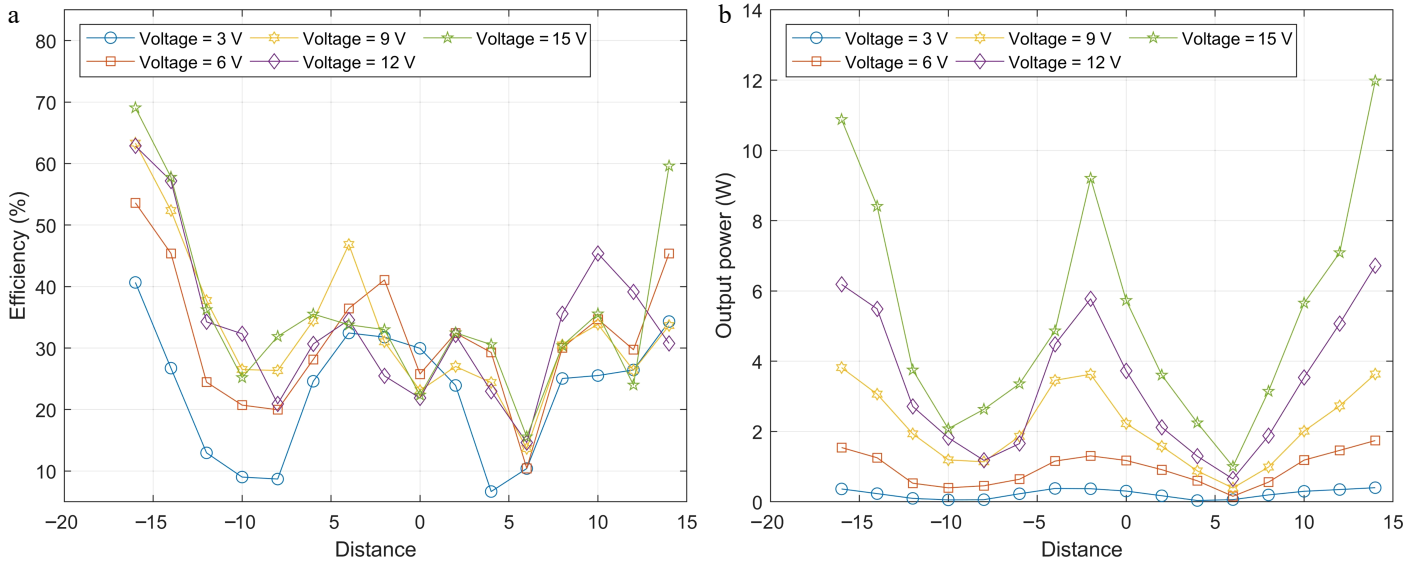

Fig. 20 (a) Efficiencies, and (b) output powers of the WPT system at different voltages in Experiment B when the shielding coil is perpendicular to the transmitting coil.

Author contributions

The authors confirm contribution to the paper as follows: conceptualization: Yang Y, Yang J; data curation: Shang S, Zhang X, Yang J; formal analysis: Yang J, Wang K; funding acquisition: Yang Y; investigation: Yang J, Shang S, Wang Y, Wang K; methodology: Yang J, Zhang X; project administration: Yang Y, Wang K, Yang J; resources: Yang Y, Zhang X, Yang J; software: Yang J, Zhang X, Wang Y; supervision: Yang Y, Wang K; validation: Yang J, Zhang X, Wang Y, Wang K; visualization: Zhang X, Wang Y; writing - original draft: Yang J; Writing - review & editing: Wang K, Yang Y. All authors reviewed the results and approved the final version of the manuscript.

Data availability

The data that support the findings of this study are available from the corresponding author upon reasonable request.

Acknowledgments

The authors are grateful for the financial support from the Ministry of Education (MoE) Academic Research Fund (AcRF) Tier-1 RG134/23 and the A*Star MTC Young Individual Research Grant (YIRG) M23M7c0115.

Conflict of interest

The authors declare that they have no conflict of interest. Yun Yang is the Editorial Board member of *Wireless Power Transfer* who was blinded from reviewing or making decisions on the manuscript. The article was subject to the journal's standard procedures, with peer-review handled independently of this Editorial Board member and the research groups.

Dates

Received 8 July 2024; Revised 15 August 2024; Accepted 4 September 2024; Published online 12 October 2024

References

1. Rong C, Wang Y, Chen M, Lu Y, Wu Z, et al. 2023. A comprehensive analysis of metamaterial-coupled WPT systems for low electromagnetic field leakage. *IEEE Transactions on Electromagnetic Compatibility* 65(1):166–76
2. Zagirnyak M, Nykyforov V, Sakun O, Chorna O. 2017. The industrial electrical equipment screened magnetic fields effect on model organisms. *2017 International Conference on Modern Electrical and Energy Systems, Kremenchuk, Ukraine, 15–17 November, 2017*. USA: IEEE. pp. 380–83. doi: 10.1109/MEES.2017.8248938

3. Zhu K, Kiourti A. 2022. A review of magnetic field emissions from the human body: sources, sensors, and uses. *IEEE Open Journal of Antennas and Propagation* 3:732–44
4. Lin K, Xu X, Zhao T, Chen SE, Braxtan N, et al. 2022. Passive Shielding Design of an Inductive Power Transfer System for Railway Applications. *2022 IEEE Transportation Electrification Conference & Expo, Anaheim, CA, USA, 15–17 June, 2022*. USA: IEEE. pp. 606–10. doi: 10.1109/ITEC53557.2022.9814018
5. Meng J, Lan H, Lu S, Cheng R, Wei R, et al. 2023. Passive magnetic shielding study for wireless power transfer system. *2023 26th International Conference on Electrical Machines and Systems, Zhuhai, China, 5–8 November, 2023*. USA: IEEE. pp. 1928-32. doi: 10.1109/ICEMS59686.2023.10344786
6. Sun X, Wei B, Li Y, Yang J. 2022. A new model for analysis of the shielding effectiveness of multilayer infinite metal meshes in a wide frequency range. *IEEE Transactions on Electromagnetic Compatibility* 64(1):102–10
7. Kvitkovic J, Patel S, Pamidi S. 2017. Magnetic shielding characteristics of hybrid high temperature superconductor/ferromagnetic material multilayer shields. *IEEE Transactions on Applied Superconductivity* 27:4700705
8. Ahn S, Hwang C, Park HH. 2014. Optimized shield design for reduction of EMF from wireless power transfer systems. *IEICE Electronics Express* 11:20130930
9. Olukotun B, Partridge JS, Bucknall RWG. 2019. Loss performance evaluation of ferrite-cored wireless power system with conductive and magnetic shields. *2019 IEEE PES Innovative Smart Grid Technologies Europe (ISGT-Europe), Bucharest, Romania, 29 September to 2 October 2019*. USA: IEEE. pp. 1–5 doi: 10.1109/ISGTEurope.2019.8905437
10. Tan L, Elnail KEI, Ju MH, Huang X. 2019. Comparative analysis and design of the shielding techniques in WPT systems for charging EVs. *Energies* 12(11):2115
11. Idris Elnait KE, Huang L, Tan L, Wang S, Wu X. 2018. Resonant reactive current shield design in WPT systems for charging EVs. *2018 IEEE PES Asia-Pacific Power and Energy Engineering Conference, Kota Kinabalu, Malaysia, 7–10 October, 2018*. USA: IEEE. pp. 56–59. doi: 10.1109/APPEEC.2018.8566600
12. Park J, Shin Y, Kim D, Park B, Ahn S. 2018. Planar Resonance Reactive Shield for Reducing the EMI in Portable WPT Device Application. *2018 IEEE Symposium on Electromagnetic Compatibility, Signal Integrity and Power Integrity, Long Beach, CA, USA, 30 July – 3 August 2018*. USA: IEEE. pp. 419–22. doi: 10.1109/EMCSI.2018.8495362
13. Pavelek M, Frivaldsky M, Spanik P. 2018. Influence of the passive shielding on the optimal working point of the wireless power transfer systems. *2018 International Symposium on Power Electronics, Electrical Drives, Automation and Motion, Amalfi, Italy, 20–22 June 2018*. USA: IEEE. pp. 773–78. doi: 10.1109/SPEEDAM.2018.8445377
14. Yan L, Gao H, Rong C, Liao Z, Xia C, et al. 2023. Efficiency Improvement of 6.78MHz Metamaterials for WPT System. *2023 26th International Conference on Electrical Machines and Systems, Zhuhai, China, 5–8 November, 2023*. USA: IEEE. pp. 3812–15. doi: 10.1109/ICEMS59686.2023.10344727
15. Hsu HM, Huang YK, Wu TL. 2019. Implementation of constant current performance of 13.56MHz Wireless Power Transfer system. *2019 IEEE Wireless Power Transfer Conference, London, UK, 18–21 June, 2019*. USA: IEEE. pp. 385–89. doi: 10.1109/WPTC45513.2019.9055703
16. Mao H, Yang B, Li Z, Song S, Zhao X. 2017. Flexible and efficient 6.78MHz wireless charging for metal-cased mobile devices using controlled resonance power architecture. *2017 IEEE Wireless Power Transfer Conference, Taipei, Taiwan, 10–12 May, 2017*. USA: IEEE. pp. 1–4. doi: 10.1109/WPT.2017.7953864
17. Xu Z, Rodriguez-Villegas E. 2022. A 6.78MHz mid-range wireless power charging system for milliwatt-power-level long-term biomedical sensing applications. *2022 IEEE Biomedical Circuits and Systems Conference, Taipei, Taiwan, 13–15 October, 2022*. USA: IEEE. pp. 270–74. doi: 10.1109/BioCAS54905.2022.9948633
18. Li K, Wu J, Wang M, Yucel AC, Hui SYR. 2023. A sandwich structure for cost-effective printed-circuit-board wireless power resonator. *2023 IEEE Applied Power Electronics Conference and Exposition, Orlando, FL, USA, 19–23 March, 2023*. USA: IEEE. pp. 818–21. doi: 10.1109/APEC43580.2023.10131590
19. Yang Y, Tan SC, Hui SYR. 2019. Communication-free control scheme for Qi-compliant Wireless Power Transfer systems. *2019 IEEE Energy Conversion Congress and Exposition, Baltimore, MD, USA, 29 September – 3 October 2019*. USA: IEEE. pp. 4955–60. doi: 10.1109/ECCE.2019.8912496
20. Yang Y, Liang HWR, Tan SC, Hui SYR. 2021. Design of a wireless power modulator for wireless power transfer systems. *2021 IEEE 12th Energy Conversion Congress & Exposition - Asia, Singapore, 24-27 May, 2021*. USA: IEEE. pp. 816-20. doi: 10.1109/ECCE-Asia49820.2021.9479411
21. Li K, Wu J, Yucel AC, Hui SYR. 2023. New Printed-Circuit-Board Resonators With High Quality Factor and Transmission Efficiency for Mega-Hertz Wireless Power Transfer Applications. *IEEE Transactions on Power Electronics* 38(10):13207–18
22. Shevchenko V, Husev O, Strzelecki R, Pakhaliuk B, Poliakov N, et al. 2019. Compensation topologies in IPT systems: standards, requirements, classification, analysis, comparison and application. *IEEE Access* 7:120559–80